atmosphere

MDPI

Article

Impact of Building Energy Mitigation Measures on Future Climate

Rabindra Pokhrel [1,*], Jorge E. Gonzalez [2], Prathap Ramamurthy [3] and Daniel Comarazamy [3]

[1] Department of Environmental Science and Engineering, Kathmandu University, Dhulikhel 45200, Nepal
[2] Environmental Sciences & Atmospheric Science Research Center, University of Albany, ETEC Building, 1220 Washington Avenue, Albany, NY 12222, USA
[3] NOAA-CREST Center, The City College of New York, New York, NY 10031, USA
* Correspondence: rabindra@ku.edu.np

Abstract: As cities are increasing technological efficacy on greenhouse gas (GH) emission reduction efforts, the surrounding urban ecosystems and natural resources may be affected by these measures. In this research, climate indicators such as heat index, extreme heat events, intensified urban heat islands (UHIs), and sea breeze are projected for the middle and end of the 21st century to understand the climate change signal on these variables with and without building energy mitigation measures. Cities amplify extreme heat and UHI impacts by concentrating large populations and critical infrastructure in relatively small areas. Here, we evaluate the combined climate and building energy mitigation impacts on localized climate metrics throughout the 21st century across extreme emission scenarios (RCP8.5) for the tropical coastal city of San Juan. The analysis of statistically downscaled global circulation model outputs shows underestimation for uncorrected summer daily maximum temperatures, leading to lower extreme heat intensity and duration projections from the present time which are corrected using bias-corrected techniques. High-resolution dynamic downscaling simulations reveal a strong dependency of changes in extreme heat events in urban settings, however, the intensities shift to lower-level grasslands and croplands with energy mitigation measures (combination of white roof, tilted photovoltaic roof, and efficient heating ventilation and air conditioning systems). The building energy mitigation measures have the potential of reducing the UHI intensities to 1 °C and 0.5 °C for the 2050 and 2100 climate periods, respectively.

Keywords: building energy; mitigation measures; climate change; future projections; extreme heat events; Puerto Rico

Citation: Pokhrel, R.; Gonzalez, J.E.; Ramamurthy, P.; Comarazamy, D. Impact of Building Energy Mitigation Measures on Future Climate. *Atmosphere* **2023**, *14*, 463. https://doi.org/10.3390/atmos14030463

Academic Editor: Jihui Yuan

Received: 14 January 2023
Revised: 21 February 2023
Accepted: 22 February 2023
Published: 26 February 2023

1. Introduction

Tropical coastal areas contain almost one-third of the total world population and are highly vulnerable to global climate change [1]. The Intra American Region (IAR) is a tropical–coastal converging zone, defined as the area enclosed by 0° N to 30° N and 100° W to 40°. The IAR region encompasses northern South America, Central America, the Gulf of Mexico, the Caribbean region, and the western Atlantic, where a complex interaction among synoptic atmospheric/oceanic patterns drives the rainfall activity in the region [2–5]. This tropical region is used in this study as a case study to assess its climatology and the relationship between rising temperatures and other environmental variables due to a global warming climate.

The vulnerability to climate change and associated extreme weather events in tropical coastal areas is directly related to accelerated Sea Surface Temperatures (SSTs) and air temperature increases [6]. In addition to higher SSTs in the IAR, the Bermuda-Azores high-pressure system (one pole of the North Atlantic Oscillation Index) interacts with the Caribbean low-level jet, causing downward dry air, hindering precipitation and warming the surface [2,7]. A clear regional warming was detected for the particular case of the IAR region for the years 1982 to 2013, where the SST had an annual trend of 0.0209 °C per

year (Glenn et al., 2015) [4] and where the air temperature is observed to be rising at a higher rate of 0.030 °C per year [6]. In addition, the Atlantic Warm Pool depicts a continuous intensification in the last decades, which in conjunction with a warmer atmosphere increases the risks for extreme temperature events. An excessively warmer atmosphere may lead to localized high-pressure ridges, which could produce heat waves or extreme heat events with potentially disastrous social, health, and economic consequences [8]. Of concern are the several definitions of heat waves and extreme heat events that have been proposed in the scientific literature [9–13]. A widely used approach considers the 97th percentile for the entire weather station data based on either heat index or temperature for two to three consecutive days [12,14,15]. Using this definition for the entire IAR region between 1980–2014, it was found that 144 extreme heat events were reported for a period of 35 years, out of which 11 events were recorded for San Juan, Puerto Rico [14]. Local records in San Juan indicate that the maximum daily temperature of 30–35 °C occurred over 14% of the time in the last 52 years, and these very warm conditions are becoming more frequent and intense [16]. For a particular documented case of San Juan, Puerto Rico, a high-pressure system induced low southeasterly winds responsible for record high summer temperatures (August 2012), leading to high rates of mortality related to heat stroke and cardiovascular diseases [17]. Extreme heat events in general expose elderly populations and people without air conditioning units to high-risk vulnerability. For the IAR region, a heat wave projection for the 21st century was conducted using a general circulation model (GCM) for different climate change scenarios, indicating an increase in both frequency and intensities [15]. Though this model is useful for evaluating global- and continental-scale climate impacts, the coarser resolution (~100 km) limits its potential to represent regional and local significant processes due to complex elevation, coastlines, and heterogeneity in land cover land use (LCLU) as well as finer-scale atmospheric process (e.g., anthropogenic feedback, clouds, and convection). A general question for urban regions, especially in the tropics, is how different climate indices (especially extreme heat events, urban heat islands, and heat index) are represented along with other environmental variables such as humidity and winds for an extreme climate change scenario. One can further ask the role of mitigation measures adopted to combat climate change impacts on urban areas and their surrounding LCLU.

LCLU in urban surfaces generates feedback between the land and atmosphere that can exacerbate extreme heat event conditions in densely populated cities. For example, Li and Bou-Zeid, 2013 [18], found UHI intensification in Baltimore, MD, while Ramamurthy et al., 2017 [19], found the NYC UHI reaching up to 10 °C during the summer of 2016, both attributing synergistic interactions between extreme heat events and urban surfaces to low evapotranspiration over cities, high anthropogenic heat, large thermal mass of buildings and paved materials, low wind speed, and air pollution. Li et al., 2016 [20], found enhancement of the Beijing Metropolitan Area UHI due to wind profile changes (both speed and direction) during heat waves, similar to results from Founda and Santamouris, 2017 [21], who found UHI intensification in Athens, Greece, to be highly dependent on wind profiles, especially low wind speed and changes in wind directions. Others have found evidence of UHI intensification during extreme heat in Madison, WI (reaching 1.80 °C during the day and 5.3 °C during night; [22]). However, Scott et al., 2018 [23], showed in total of 54 US cities with daily observation records for 15 years (2000–2015) that in most of the cities analyzed, rural temperatures increased faster than urban temperatures, leading to lower UHI magnitudes during extremely hot days. As a result, active responses to the UHI phenomenon are highly and urgently required not only to improve outdoor thermal comfort but also the indoor environment [24]. This underscores the need for studies underlying land surface processes that could determine how UHIs vary over coastal cities (Caribbean in this case) and how could they be mitigated in a future changing climate.

Consequently, policies and programs addressing mitigation due to rapidly increasing temperatures are rapidly growing in Latin America and the Caribbean [25,26]. The United Nations Environmental Program (UNEP), through its Economic Commission for Latin America and the Caribbean studies (ECLAC), has demonstrated that renewable energy

sources would play an essential role in these regions contributing to improving the inhabitant quality of life. UNEP and the World Bank have several projects dealing with mitigating climate change in regional areas, where 31% correspond to the efficient use of energy and promotion of renewable energy sources [25]. Aggressive policies aimed at upgrading only heating/cooling systems and appliances could result in decreased electricity use as low as 28%, potentially avoiding the installation of new-generation capacity [27] that could have a positive impact on the quality of the urban climate. A recent study highlights that the built environment of the future would transform buildings into resource assets—fully self-aware, adaptive, and with two-way communication with the electric grid (to optimize operating cost)—and add market value to the assets [7]. In addition to this, the stricter de-carbonization regulation would open doors to innovative designs and renewable energy integration in all building sectors of urban regions. The free space available on rooftops used with the full potential for energy services could achieve the de-carbonization goals and increase the building value. For city-scale deployment, different types of roof applications (cool roof, green roof, and photovoltaic roof) on buildings have shown to reduce air temperature and energy consumption [28–34]. One such application is rooftop photovoltaic installations, which decrease the temperature and urban heat island (UHI) effects [28,35], especially reducing daytime UHI and peak energy demands (Pokhrel et al., 2020) [36]. These later works show that a higher albedo of a tilted photovoltaic shaded roof can act as a radiant barrier that reflects heat from thermal radiation from the roof surface [36,37].

In this work, we evaluate the environmental impacts of mitigation options (a combination of cool roof, tilted photovoltaic roof, and efficient HVAC systems) based on the recommendations for reducing peak air conditioning demands (with a reduction potential of 33%) from earlier studies by Pokhrel et al. (2019b) [38] and Pokhrel et al. (2020) [36] for the San Juan Metropolitan Area (SJMA) of Puerto Rico. This study may also support public energy policies such as the Puerto Rico Integrated Energy Resource Plan, which aims to increase energy efficiency on the island by 25% by 2030 and the integration of renewable energy resources by 100% by 2050 (IRP, PREPA 2018–2019).

Evaluation of climate variables and energy demands at larger urban scales have either focused on the use of statistical [39,40] or process-based models [41,42]. The absence of interactions between weather and buildings is one of the limitations of these approaches and could amplify in the context of changing climate. An approach to resolve this limitation is by coupling weather prediction to Building Energy Models (BEMs) [43–45]. However, the computation cost and lack of urban morphology and its corresponding parameters have limited the studies to a few events or to short periods (<1 season). Here, we present the impacts of mitigation options on 2 m air temperature, extreme heat events, and UHI reduction potential for the dense population region of the SJMA for an extreme emission scenario for a multi-year period.

The tropical coastal region of Puerto Rico and specifically the SJMA is taken as a case study for this research. The SJMA consists of seven cities with 630 km^2 area and 1 M inhabitants. According to UN demographic projections for 2100, Puerto Rico does not have a positive or negative trend (i.e., population does not change). However, there is a transition plan in Puerto Rico from fossil-based generation to renewable energy. Puerto Rico, as most tropical island states, is very dependent on foreign resources for energy generation, and is consequently sensitive to global fluctuations in fuel costs. The island's generating capacity is 4879 MW, comprising 2892 MW of steam-electric, 846 MW of combustion-turbine capacity, 1032 MW of combined cycle capacity, 100 MW of hydroelectric capacity, and 9 MW of diesel capacity. All steam turbines are oil- (2500 MW) or coal-based (450 MW) (fortieth annual report, PREPA 2013) [46]. Thus, more than 80% of the energy production is based on oil (75%) and natural gas (15%). The dependency on fossil fuel for energy production and the inefficiency in the electrical energy infrastructure can be viewed as a factor for the high electricity rates of more than USD 0.25/kWh, one of the highest of any US state or territory. Furthermore, the service sector of the economy of Puerto Rico is very large, reflected in large components of the residential (40%) and commercial customers (51%) in the island,

with more than 90% of annual energy sales to these sectors alone from a total of 16,000 GWh in 2016 (https://www.aeepr.com/INVESTORS/Default.aspx, accessed on 15 January 2023). Most of the energy used in the residential and commercial sectors is in air conditioning to maintain human comfort in the building sector [47] (Reddy et al., 2016), a common factor for most tropical coastal cities, where air conditioning can often exceed 50% of the total energy budget [48]. According to the Final Integrated Resource Plan (IRP) approved by Puerto Rico Energy Bureau (PREB) on August 2020, 3500 MW of new power should come from solar power with 1360 MW of battery energy storage by 2025, and energy efficiency and demand respond programs should be introduced to reduce the demand of commercial and industrial sectors by 2% every year. Furthermore, the IRP has plans of introducing 100% power with renewables by 2050 (https://energia.pr.gov/en/preb-approved-irp-2, accessed on 15 January 2023). The key science questions this study attempts to answer are as follows: how are extreme temperature events projected under a warming climate, and what may be the role of energy mitigation measures (solar) on environmental sustainability under a warming climate for a tropical coastal city?

The organization of the manuscript following this Introduction focuses on methods on data used (GCM ensemble), point-based statistical downscaling for the SJMA, and modeling with dynamic downscaling. The results are categorized with extreme heat event projections, in addition to the presentation of dynamic downscaling results for underlying land surface processes that change with and without mitigation measures for the future climate change scenario.

2. Methodology

2.1. GCM Ensemble

This study explores impacts of building energy mitigation options in a warming climate. For this, two approaches are used: single-point projections and dynamic downscaling techniques. For single-point projections, ensemble members of GCMs are used belonging to the Fifth Climate Model Inter-comparison Project (CMIP5; Taylor et al., 2012) [49] and are detailed in Table 1. For each model, we considered daily maximum temperature between 2006 and 2100. Two scenarios are considered based on the representative concentration pathways [50], RCP4.5 and RCP8.5, which use a combination of global policies, technologies, and demographic projections to estimate global radiative forcing paths. RCP4.5 is considered a medium-emission scenario, with increasing global radiative forcing that stabilizes by 2100 at 4.5 W/m^2. RCP8.5 is a high-emission or "business as usual" scenario, with increasing radiative forcing reaching around 8.5 W/m^2 by end of century.

2.2. Statistical Bias Correction (SBC)

For single-point projections, ensemble members of GCMs for temperature records are further bias-corrected for mean and standard deviations for a reference point, in this case the San Juan International Airport (SJIA). These historical records of the SJIA were in turn used to perform bias correction GCM projections following the work of Piani et al., 2010 [51], and Hawkins et al., 2013 [52]. The bias correction technique corrects for model mean and standard deviation using a linear model.

$$T_{BC} = \overline{T}_{\text{obs,REF}} + \frac{\sigma_{\text{obs,REF}}}{\sigma_{\text{GCM,REF}}}\left(T_{\text{GCM,RAW}}(t) - \overline{T}_{\text{GCM,REF}}\right) \quad (1)$$

Here, T refers to the temperature records and σ refers to its standard deviation. Subscripts obs and GCM refer to observation and model data, respectively, while REF and RAW refer to the reference (2008–2017) and entire projection periods (2006–2100). The over bar ($\overline{\ }$) marker denotes use of the average for the specified dataset and time period. For all models, the geographically closest land grid point to the SJIA was used to develop all projections. A single point is used due to GCMs' generally coarse resolution, meaning that other grid points might be too distant from SJIA to provide relevant information.

Table 1. Twenty-five-model ensemble and center of origin used in single-point heat wave projections based on location of SJIA (18.3522 lat.° × −66.1186 lon.°).

Center	Model	Resolution (lat.° × lon.°)	Selected Coordinates (lat.° × lon.°)
Commonwealth Scientific and Industrial Research Organization: Bureau of Meteorology (Australia)	ACCESS1.0 ACCESS1.3	1.25 × 1.875 1.25 × 1.875	18.75 × −63.75 18.5 × −66
Canadian Centre for Climate Modeling and Analysis (Canada)	CanESM2	2.7906 × 2.8125	18.139 × −67.5
National Center for Atmospheric Research (United States)	CCSM4	0.9424 × 1.25	18.376 × −66.25
Centro Euro-Mediterraneo per i Cambiamenti Climatici (Italy)	CMCC-CMS	3.7111 × 3.75	17.72 × −65.625
Centre National de Recherches Météorologiques/Centre Européen de Recherche et de Formation Avencée en Calcul Scientifique (France)	CNRM-CM5	1.4008 × 1.40625	18.911 × −66.094
Commonwealth Scientific and Industrial Research Organization/Queensland Climate Change Centre of Excellence (Australia)	CSIRO-Mk3.6.0	1.8653 × 1.875	17.72 × −66.25
NOAA Geophysical Fluid Dynamics Laboratory (United States)	GFDL-ESM2G GFDL-ESM2M	2.0225 × 2 2.0225 × 2	19.214 × −66.25 19.214 × −66.25
NASA Goddard Institute for Space Studies (United States)	GISS-CM3 GISS-E2-H GISS-E2-R	2 × 2.5 2 × 2.5 2 × 2.5	19 × 66.25 19 × 66.25 19 × 66.25
Met Office Hadley Centre (UK)	HadGEM2-AO HadGEM2-CC HadGEM2-ES	1.25 × 1.875 1.25 × 1.875 1.25 × 1.875	18.75 × −66.625 18.75 × 66.625 18.75 × 66.625
Institut Pierre Simon Laplace (France)	IPSL-CM5A-LR IPSL-CM5A-MR IPSL-CM5B-LR	1.8947 × 3.75 1.2676 × 2.5 1.8946 × 3.75	18 × −67.5 17.7464 × −65 18 × −67.5
Japan Agency for Marine-Earth Science and Technology, Atmosphere and Ocean Research Institute/National Institute for Environmental Studies/Japan Agency for Marine-Earth Science and Technology (Japan)	MIROC-ESM MIROC-ESM-CHEM MIROC5	2.7906 × 2.8125 2.7906 × 2.8125 1.4008 × 1.40625	18.13897 × −67.5 18.13897 × −67.5 18.91036 × −66.0938
Max Planck Institute for Technology (Germany)	MPI-ESM-LR MPI-ESM-MR	1.8653 × 1.875 1.8653 × 1.875	17.71996 × −65.625 17.71996 × −65.625
Meteorological Research Institute (Japan)	MRI-CGCM3	1.12148 × 1.125	18.50458 × −66.375
Institute for Numerical Mathematics (Russia)	MRI-CGCM3	1.5 × 2	18.75 × −66

2.3. Dynamic Downscaling for Future Climate Change

The results from statistical downscaling were used and served as a reference to carry out dynamic downscaling providing key periods to simulate, referred to here as time slices, in addition to additional advantages of a dynamic downscaling effort. The flow chart, which describes this study's overall methodology for future climate projections (including statistical and dynamic downscaling), is illustrated in Figure 1. Point-based projections for temperatures were used to forecast long-term projections of these variables until 2100, which guides the more detailed projections. As indicated before, for detailed projections, this study uses a high-resolution configuration of the urbanized WRF model coupled with a modified multi-layer urban canopy and BEM parametrization as a tool to study changes in environmental variables under climate change conditions. The bias-corrected runs of the Community Earth Systems Model version 1 (CESM1) (Bruyere et al., 2014) [53] datasets were used as initial and boundary conditions at a horizontal resolution 0.94 latitude × 1.24 longitude. The regional-scale biases due to having coarse spatial resolution and limited representation of some physical processes were corrected in CESM1 with the bias correction method developed by Bruyere et al. (2015) [53]. Their work adjusts CESM outputs by combining a 25-year (1981–2005) mean annual cycle from ERA-Interim reanalysis and a 6-hour perturbation term representing the climate signal. The

bias correction removes the mean annual bias while retaining the day-to-day climate variability from CESM as follows:

$$\mathrm{CESM_{BC}} = \mathrm{ERAI(mean)} + \mathrm{CESM'} \quad (2)$$

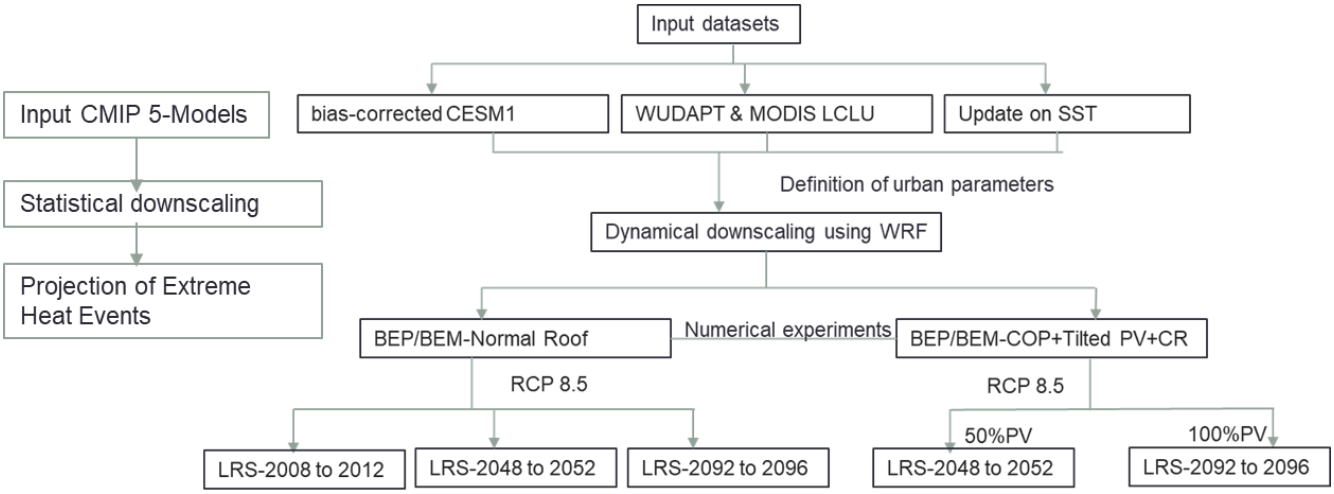

Figure 1. The overall methodology adopted in this study.

Regional modeling forced with bias-corrected CESM was shown to improve results (Bruyere et al., 2014) [53]. Specifically, the air temperatures over the Caribbean region showed a deceased cold bias when all boundary condition variables were corrected with reanalysis data. Sea Surface Temperatures from bias-corrected CESM are updated daily.

High-resolution regional climate models have been used to improve the representation of precipitation and temperature [54,55], especially in locations where complex surface processes are significant (e.g., mountains, coasts, and cities), although some studies have found geographically inconsistent accuracy improvements [56]. In addition, high-resolution dynamic downscaling methods are used to derive projections of extreme events, such as heat waves (Gao et al., 2012 [57]; Ortiz et al., 2019 [58]). Here, we employ advances in the representation of urban physics in the WRF model to project heat wave metrics and building energy throughout the SJMA. Our simulation approach focuses on three time periods representing historic (2008–2012), mid-century (2048–2052), and end of the century (2092–2096) and for the late rainfall season (LRS) only. We chose the LRS (August–November) as it is a period where extreme heat events are more evident for the San Juan Metropolitan Area [38] (Pokhrel et al., 2019a).

The simulation covers two sets of experiments: normal conditions and building energy mitigation alternatives. The normal condition represents normal roof conditions, as in BEMs, and mitigation alternatives cover a combination of building-integrated active and passive systems such as cool roof (albedo changed to 0.7 from 0.15), higher Coefficient of Performance (COP increase to 3.5 from 3), and addition of tilted solar photovoltaic roofs (PV) (50% of roof area for mid-century and 100% of roof area for end-century) based on their reduction potential for the same region. The passive building-integrated mitigation options considered here have previously been studied [38]. For a roof with tilted PV panels, the approach follows work from a recent study by Pokhrel et al. (2020) [36], where the building roof temperature of the BEM was adjusted using modifications based on the energy balance of roofs including tilted PV panels. All numerical experiments were assessed by maintaining all land surface morphologies as of 2008–2012, which consist of World Urban Database Access Portal Tool (WUDAPT) Land Class Zones (LCZs) for urban classes and MODIS LCLU for natural classes. The domain configurations for dynamic downscaling and LCLU for the finer domain are presented in Figure 2.

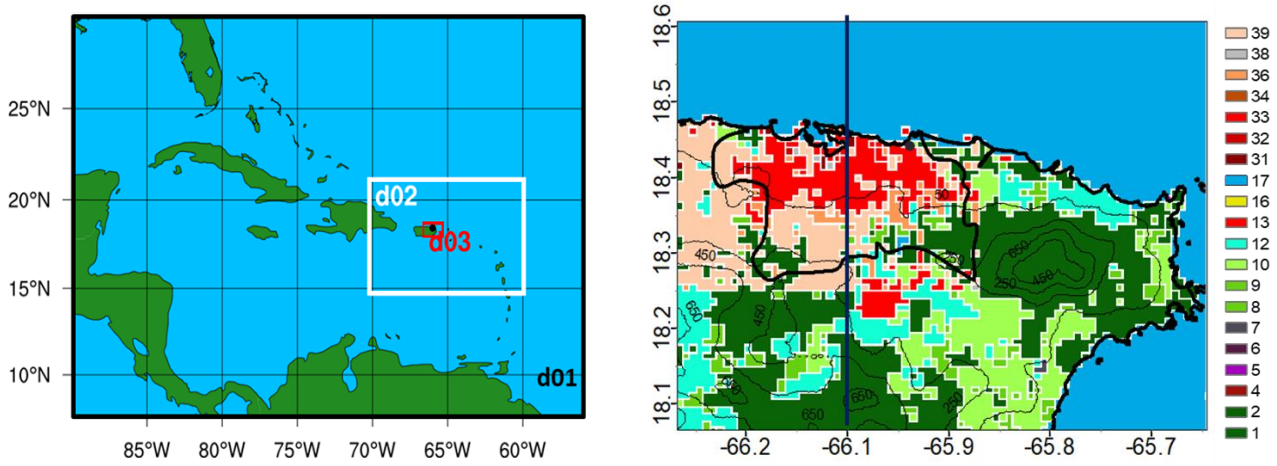

Figure 2. WRF domain configuration (**left**) and finer domain configuration. d01 (whole figure), d02 (white box), d03 (red box) corresponds to domain 1, 2 and 3. (**right**) with MODIS LCLU for natural classes and WUDAPT LCZs for urban classes (2—evergreen broad leaf forest, 17—water, and 33—compact low rise). The vertical black line shows the cross-section passing through −66.1° lon.

3. Results

3.1. Impacts of Climate Change: GCM Ensemble of SBC (Static Bias Correction) Projections

This section details the possible impacts of climate change on extreme heat events for the SJMA. We apply the bias correction technique outlined in Section 2 [52] to downscale each model in a 25-member ensemble which reveals significant cold biases in raw GCM output for the SJIA daily maximum temperature records. We use Kernel density estimates of daily maximum temperatures for each ensemble member to quantify the impact of the statistical downscaling technique on mean and standard deviation statistics. As shown in Figure 3, models without bias correction generally underestimate observations by an average of 5 °C. This may be partly due to SJIA's proximity to the ocean, which is included in more of the GCM's grid cell area. The statistical downscaling technique modifies each ensemble member's distribution to match that of the station observations more closely. In addition, inter-model spread in mean and standard deviation is reduced during the reference period for the bias-corrected GCM.

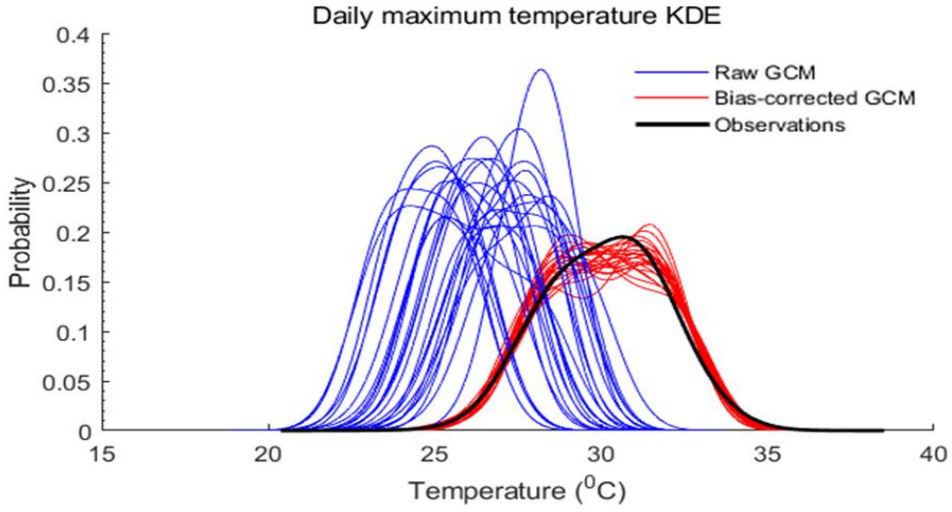

Figure 3. Daily maximum temperature KDE with raw GCM (25-model ensemble), with bias-corrected GCM and observation record for SJIA.

Bias-corrected and uncorrected mean daily maximum temperatures are shown in Figure 4a,b, showing a nearly linear trend in both the high-emission scenario (RCP8.5) and

stabilization scenario (RCP4.5). RCP4.5 shows a linear trend of 0.1778 °C/decade, while RCP8.5 grows twice as fast, 0.3555 °C/decade, for the raw GCM. The bias-corrected GCM increases at a rate of 0.5 °C/decade and 0.233 °C/decade for the RCP8.5 and RCP4.5 scenarios, respectively. Model spread, quantified as 95% confidence intervals, becomes slightly wider towards the latter half of the century; however, both scenarios show significant changes only after the middle of the century.

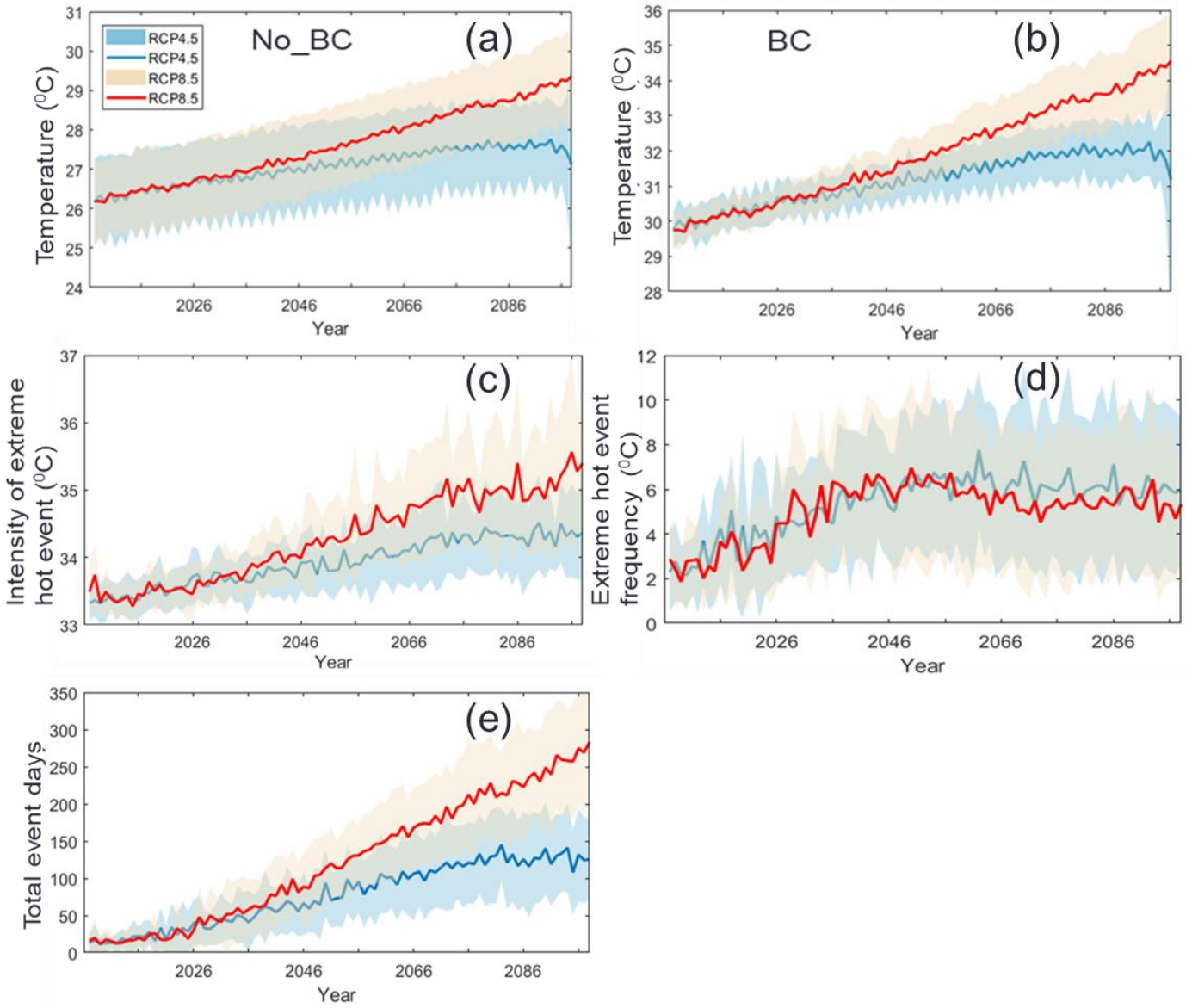

Figure 4. Daily maximum temperature and extreme heat event metric projections for SJMA. Top row (**a**,**b**) shows bias-corrected and uncorrected projections of daily maximum temperature; mid-row (**c**) shows mean heat wave intensity (bias-corrected) and mean heat wave frequency (**d**) (bias-corrected). Bottom row (**e**) shows the total extreme hot days per year. Solid blue and red bands indicate the 25-model ensemble mean, with shaded bands representing bootstrapped 95% confidence intervals.

Bias-corrected mean intensity, defined as the mean of extreme heat events that represent the 95th percentile (32.8 °C) for three consecutive days (Figure 4c), grows at a rate of nearly 0.222 °C (RCP8.5) per decade, while the uncorrected record grows at 0.1 °C/decade, more than two times slower. Mean extreme heat event frequency (Figure 4d) increases at a similar rate for both scenarios until the middle of the century, increasing from two to six events; however, event frequency remains constant after 2050 mainly due to the increase in total duration (days) of the events (Figure 4e). The total event duration records that

extreme heat events would last longer and increase at a rate of 3 days/year for RCP8.5, higher by more than two times (1.222 days/year) as compared to RCP4.5. Towards the end of century there are more hot days for the RCP8.5 scenario (Figure 4e). This is due to both usage of a limited window for hot events to happen (i.e., August–November) as well as a constant temperature threshold for the event. As mean daily temperatures surpass 32.8 °C by the early 2060s, the likelihood of any given day surpassing this temperature increases. This might lead to separate events "consolidating" into longer-lasting extreme heat events. It also explains why changes in this metric are much lower in uncorrected data (Figure 4a), as temperatures are less likely to reach the extreme heat event threshold. These results compare favorably with the 26-model ensemble used in the projections of heat wave events for New York City [58], which corrects for the mean of the temperature distribution and standard deviations. The bias correction technique to downscale temperatures from the GCM to the local scale reduces differences between observation records by reducing biases in both the mean and variance of the model. Applying the technique to each model in the 26-member ensemble results in a reduction, in general, of inter-model spread, as all models are downscaled to the same historical record. One limitation of this approach is the assumption that the relationship between observations and GCM output will remain stationary for the entire projection period, which might not account for feedback processes such as additional anthropogenic heat and soil desiccation or moistening. In addition, the coarser spatial resolutions of GCM and limitations of availability of different variables from weather stations limits the application of statistical downscaling.

To partially address some of these limitations, we conducted a set of simulations using urban WRF, considered a state-of-the-art high-resolution urbanized regional climate model. This dynamic downscaling effort incorporates most of the urban surface–atmosphere feedbacks that may modify extreme heat event conditions, rather than statistical relationships developed or assumptions about the stationarity of bias correction parameters. These assumptions are particularly relevant for projections in the SJMA, as it has been shown that the stationarity assumption may be violated in coastlines and especially in warm projections [59], where grid cells may contain water, which in turn modifies near-surface temperatures. The results from statistical downscaling with and without bias correction shows that the temperature starts to change from mid-century (2050) for both RCP4.5 and RCP8.5. In addition, towards the end of century RCP8.5 presents a maximum rise in daily maximum temperature. These results guide us to choose RCP8.5 for mid- and end-century dynamic downscaling.

3.2. Dynamic Downscaling Model Validation

Historical period simulations (in this case urbanized WRF) were evaluated against the San Juan International airport (SJIA) station for daily maximum temperature, relative humidity, and wind speed for the reference historical period of 2008–2012 (Figure 5). Simulated results were compared against Kernel density estimates (KDE), an approximation of a dataset's distribution. The airport station reported a mean daily maximum of 27.6 °C with a standard deviation of 3.59 °C. WRF simulations results, interpolated using nearest neighbor, showed a mean daily maximum of 26.9 °C (2.5% error) with 3.84 °C standard deviation (7% error). These results are consistent with Ortiz et al. (2019) [58], who found less than 1% and 10% error on the mean of daily maximum temperatures and standard deviation, respectively. Relative humidity, in general, was underestimated in the WRF simulation for values less than 40% and higher than 80%. The bimodal nature of the relative humidity is observed in weather stations at 73 and 82%. The bimodal nature is captured in the WRF simulation at 57 and 73%. Wind speeds for both the observation and simulation have a mean of 4.8 m/s; however, the maximum wind speed is underestimated by the simulation for values higher than 8 m/s by 1 to 1.5 m/s. The simulated maximum wind speed of 15 m/s compares with 23 m/s from the observation.

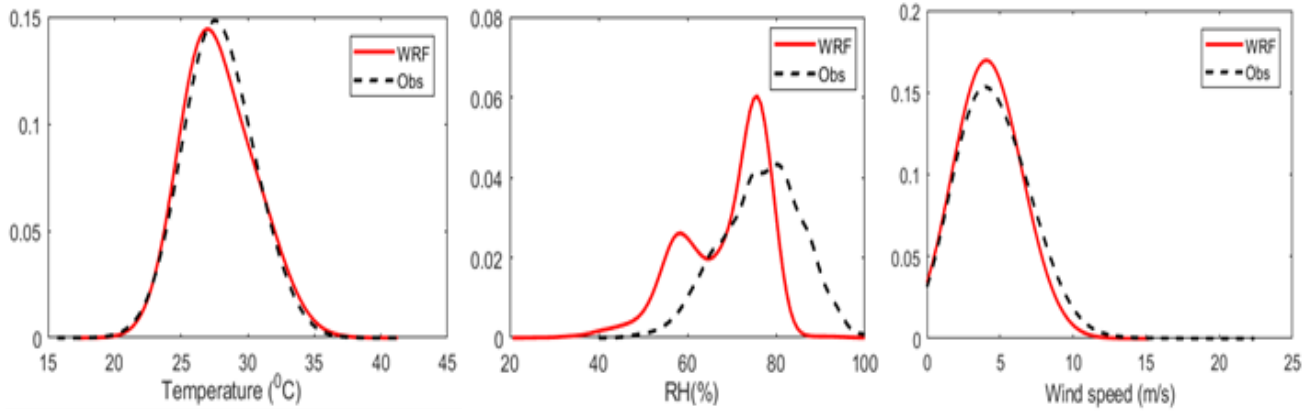

Figure 5. Kernel density estimates of (**left**) daily maximum temperature, (**middle**) relative humidity, and (**right**) wind for historical simulation period (2008–2012) for every LRS for observations and WRF simulation.

3.3. Dynamic Downscaling Model Results for Climate Change Impacts on Extreme Heat Events

The impact of climate change on extreme heat events and on other environmental variables for the middle of the century and end of the century are evaluated in this section. The simulation results are evaluated with and without building energy mitigation measures. Building energy mitigation options are those that are discussed in Section 2, and include a combination of white roof, tilted PV roof, and efficient HVAC systems (higher COP). Mean extreme heat event intensity (Figure 6) projections show that more significant increases are closer to the coast and in the metropolitan region than inland locations. Dynamic downscaling without any building energy mitigation measures for the middle of the century (2048–2052; 2050) and the end of the century (2092–2096; 2100) results in increases in the extreme heat event intensities to 35 °C and 35.5 °C, respectively, for the central urban location of the SJMA, similar to results in the statistically downscaled projections. The maximum intensity is simulated at the core of the city, inland to the coast at lower elevations where the dominant land category is compact low rise. At locations southeast of the SJIA where the dominant LCLU is cropland and grassland, the intensity is as high as 34 °C, higher than the threshold of 32.2 °C by 1.8 °C. Intensity, simulated to mitigate extreme temperature events, reduces the impact on the metropolitan region. Results for 2050 and 2100 with building energy mitigation measures reduce the event intensity by 1 °C and 1.5 °C in urban centers, whereas the maximum intensity simulated to shift towards low-level cropland and grassland LCLU close to the southeast and south of the SJIA. As cities increase efficacy on greenhouse gas emission reduction efforts, the surrounding ecosystems and natural resources close to urbanization might be affected by climate system changes and variability. Thus, it is essential to find a balance so that the impacts on ecosystems could be minimized. Here, the building energy mitigation options have a net result of decreasing the UHI, with a dual positive impact of mitigating climate change impacts and reducing greenhouse gases.

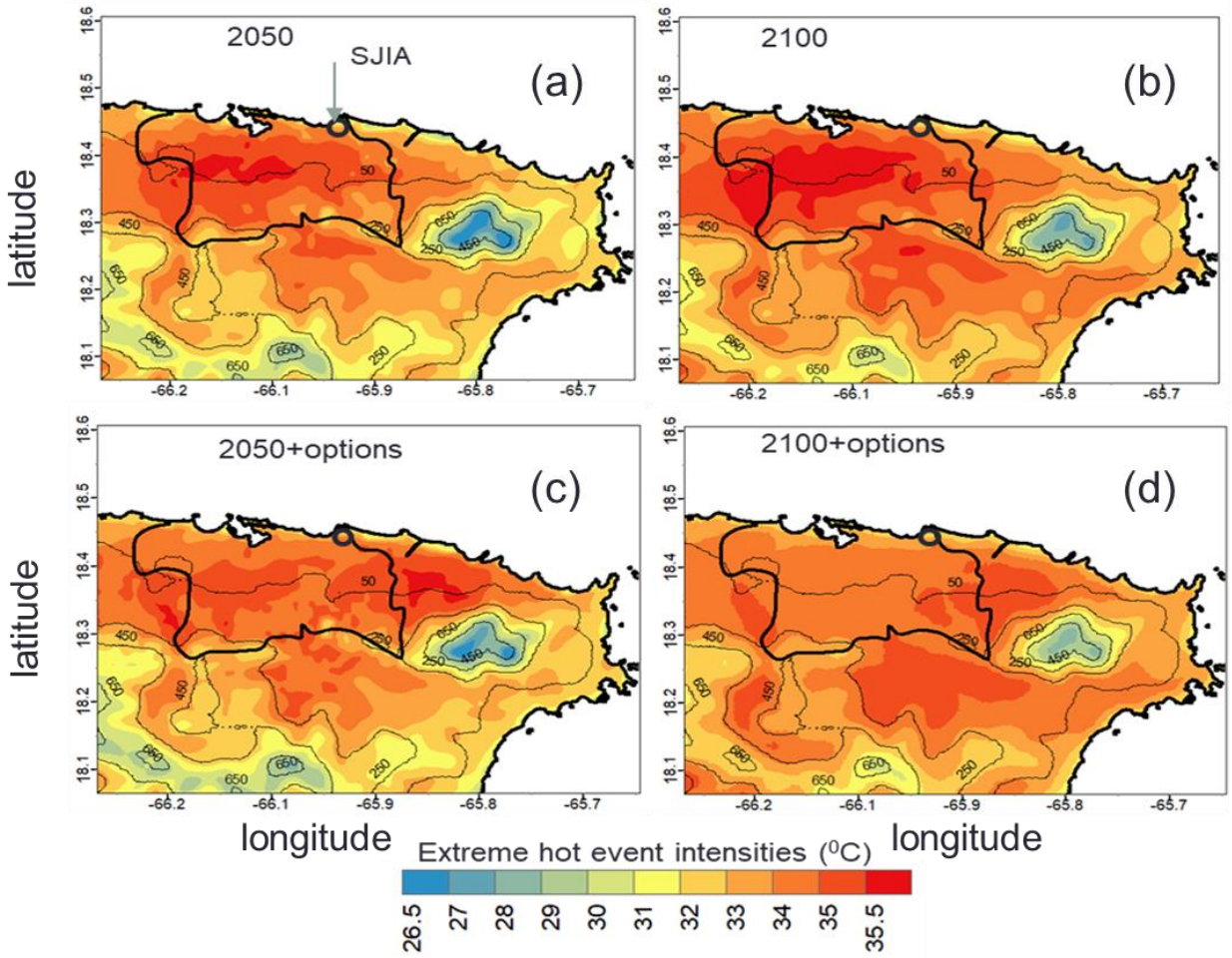

Figure 6. Extreme heat event intensities (representing greater than 95%, i.e., >32.8 °C) for middle of century and end of century with and without energy mitigation measures. (**a**) Extreme heat event intensity for 95% for 2050 (**b**) for 2100 (**c**) 2050 with energy mitigation options (**d**) for 2100 with mitigation measures.

3.4. Dynamic Downscaling Model Results for Climate Change Impacts on Heat Index

Relative humidity (RH), which measures the saturation of the atmosphere to water vapor, is projected to increase in all cases (or scenarios). Relative humidity in combination with air temperature provides information on heat index, which is an important consideration that determines how hot the body feels when exposed to ambient conditions, and this index has also been used to study extreme heat events for the Caribbean region [14,15]. Studies have shown that the water vapor content of air, in addition to ambient temperature, regulates the ability of humans to cool down via evaporation of sweat. In the business-as-usual scenario, the RH anomalies (Figure 7; left panel) without mitigation measures for the middle and end of the century show increments. For 2050 there is no change along the coast, however, at urban centers, a positive increase of 2.5% is simulated. For 2100 the anomalies are uniform, of 2.5 to 5%. As RH follows the temperature trend, the anomalies are lower for the higher temperature of 2100 compared to 2050. The mitigation measures increase RH in the metropolitan region, ranging from a 17.5% to 20% increase from historic periods. For tropical coastal cities, extreme heat wave events are defined based on heat index, which is an essential consideration for human health and comfort. The projection of heat index anomalies (Figure 8) indicates increases in all periods, reaching 5% by 2050 and 7.5% by 2100 in the SJMA. The mitigating measures reduce the heat index by 2.5% over urban centers by 2050; however, it increases to 7.5% by the end of the century.

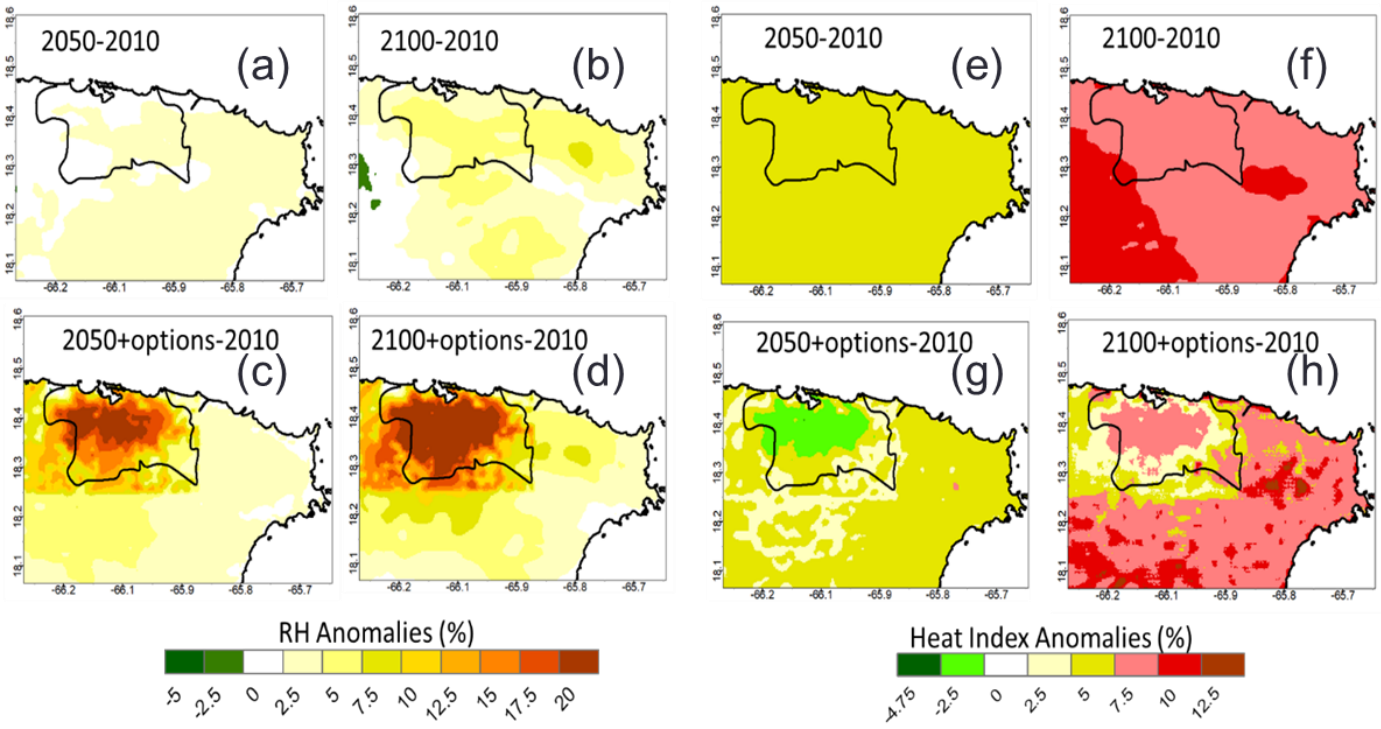

Figure 7. Relative humidity (RH) anomalies for 2050 (**a**) RH anomalies for 2100 (**b**) and RH anomalies with mitigation option for 2050 (**c**,**d**) RH anomalies with mitigation option 2100; Heat index anomalies for 2050 (**e**) 2100 (**f**) and heat index anomalies for 2050 with mitigation options (**g**) and heat index anomalies for 2100 with mitigation options 2100 (**h**).

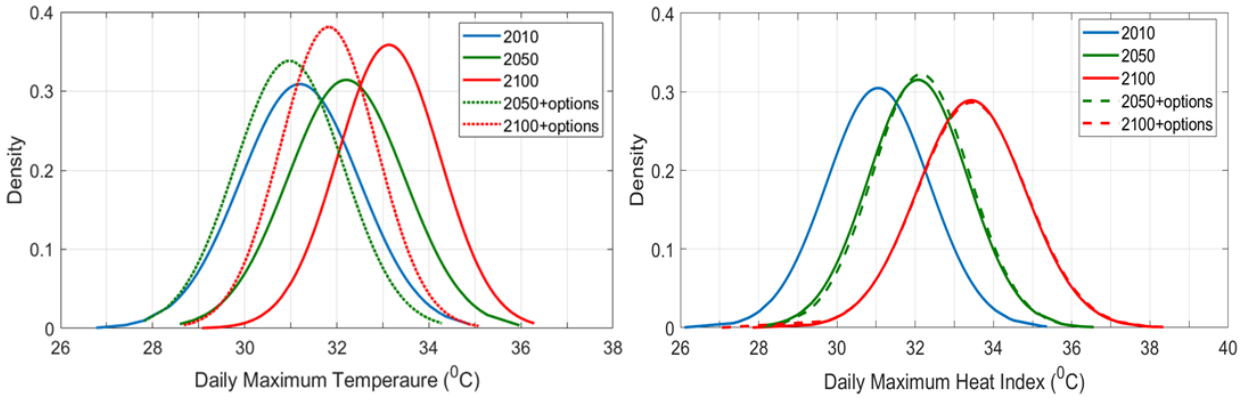

Figure 8. PDF of mean daily maximum temperature (**left**) and mean peak heat index (**right**) for the densely packed region of SJMA.

The probability density function of daily maximum temperature and daily maximum heat index for the densely packed region of the SJMA are presented in Figure 8. The mean daily maximum temperatures are 31.2 °C, 32.3 °C, and 33.3 °C, respectively, for historic, mid-century, and end-of-century periods. However, the building energy mitigation measures reduce the mean to 31 °C and 31.8 °C with a reduction potential of 2.3 °C and 1.5 °C for 2050 and 2100, respectively. The tail of distribution for 2050 has a reduction potential of 0.8 °C from historic periods. Comparison of the tail of distributions from 2050 and 2100 with and without mitigation measures shows a reduction potential of 1.8 °C and 1.2 °C simultaneously, indicating a reduction in extreme heat events. The daily maximum heat index also shows the same reduction potential for the mean distribution without building energy mitigation measures. However, the distribution does not indicate any significant improvements when compared with and without mitigation measures. This

is mainly due to the proportional increase in relative humidity coinciding with the decrease in temperature throughout the SJMA.

3.5. Model Results for Climate Change Impacts on the Boundary Layer

In order to study the boundary layer profile variation for mid- and end-century periods with and without building energy mitigation measures, air temperature (contour lines in °C) is plotted with horizontal wind vectors and shaded contours for vertical wind are shown in Figure 9 for the historic period at 18 UTC and 10 UTC. From Figure 9 it is noticed that the temperature in the upper atmosphere for topography greater than 600 m does not change significantly between both 18 and 10 UTPC. However, the horizontal wind speed near the surface (elevation < 200 m) is simulated to be greater than 2–3 °C for 18 UTC, and also the horizontal wind speed is greater for this region especially due to the influence of sea breeze. Vertical upward convective motion is seen to be maximum during afternoon in the urban region, and a circulation is simulated between urban locations and the nearby ocean. However, during the morning hour (10 UTC), vertical motion is noticed at higher elevation (>400 m) over the land with much higher wind speed as compared to the urban region and nearby ocean, and circulation is seen over this topography with higher horizontal wind speed.

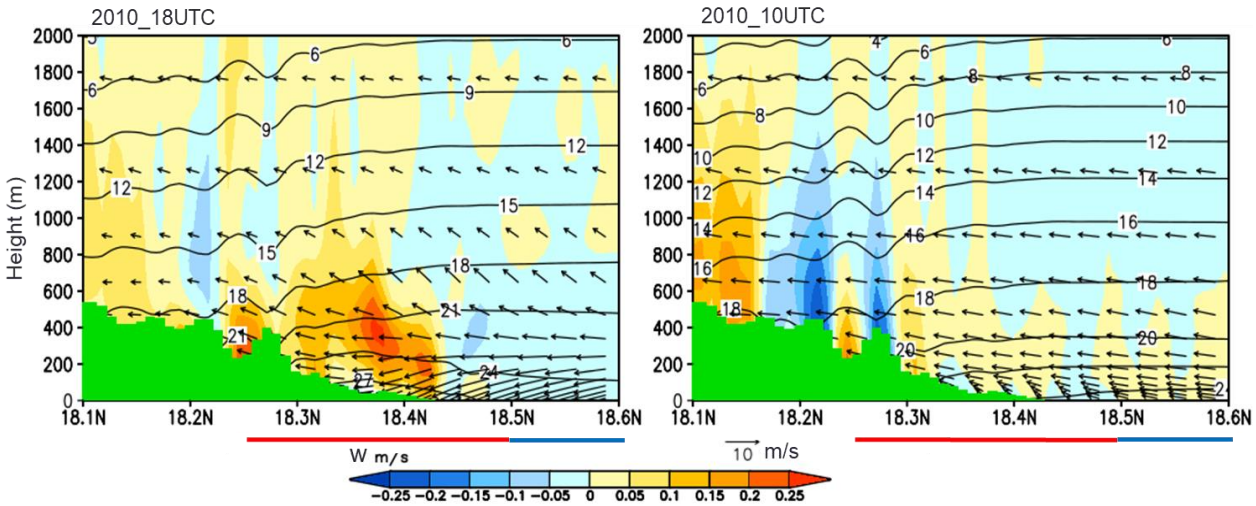

Figure 9. Temperature profile (contour lines), horizontal wind vector, and shaded contour of vertical wind (W in m/s) for mean of 18 UTC (2 PM LST) (**left**) and 10 UTC (6 AM LST) (**right**). The red line represents urban locations and blue line delineates ocean. The blue colors represent downward vertical motion, whereas the yellow–red shows upward vertical motion. The green filled solid line represents topography.

In addition to the historic period analysis of the boundary layer, the influence of climate change with and without building energy mitigation measures is studied to learn of any significant impacts on the vertical structure of the temperature, the wind speed, and convective circulation for 2 PM LST (Figure 10). For this reason, Figure 10 shows a temperature (contour lines) and horizontal wind vector difference for the middle and end of the century with the historic period in addition to the vertical wind (W) as a shaded contour. From the figure it is noticed that the climate change impacts increase the near-surface urban air temperature from 0.9 to 1.1 °C for 2050 and 1.8–2 °C by 2100, respectively, as compared to the historic period. The horizontal wind speed just over the urban region is seen to decrease by 0.5 m/s and 1–1.5 m/s for 2050 and 2100, respectively. The vertical wind circulation for 2050 and 2100 without building energy mitigation measures does not show any noticeable difference, despite the high difference in mean maximum temperature. This is mainly because of the high reduction in wind speed for 2100 as compared to 2050, which fails to produce a significant change in vertical wind speed. Energy mitigation measures do not show significant differences in temperature over the entire region, except over the

urban region where 0–0.3 °C and 1 °C increases are noticed for the 2050 and 2100 periods as compared to the historic period.

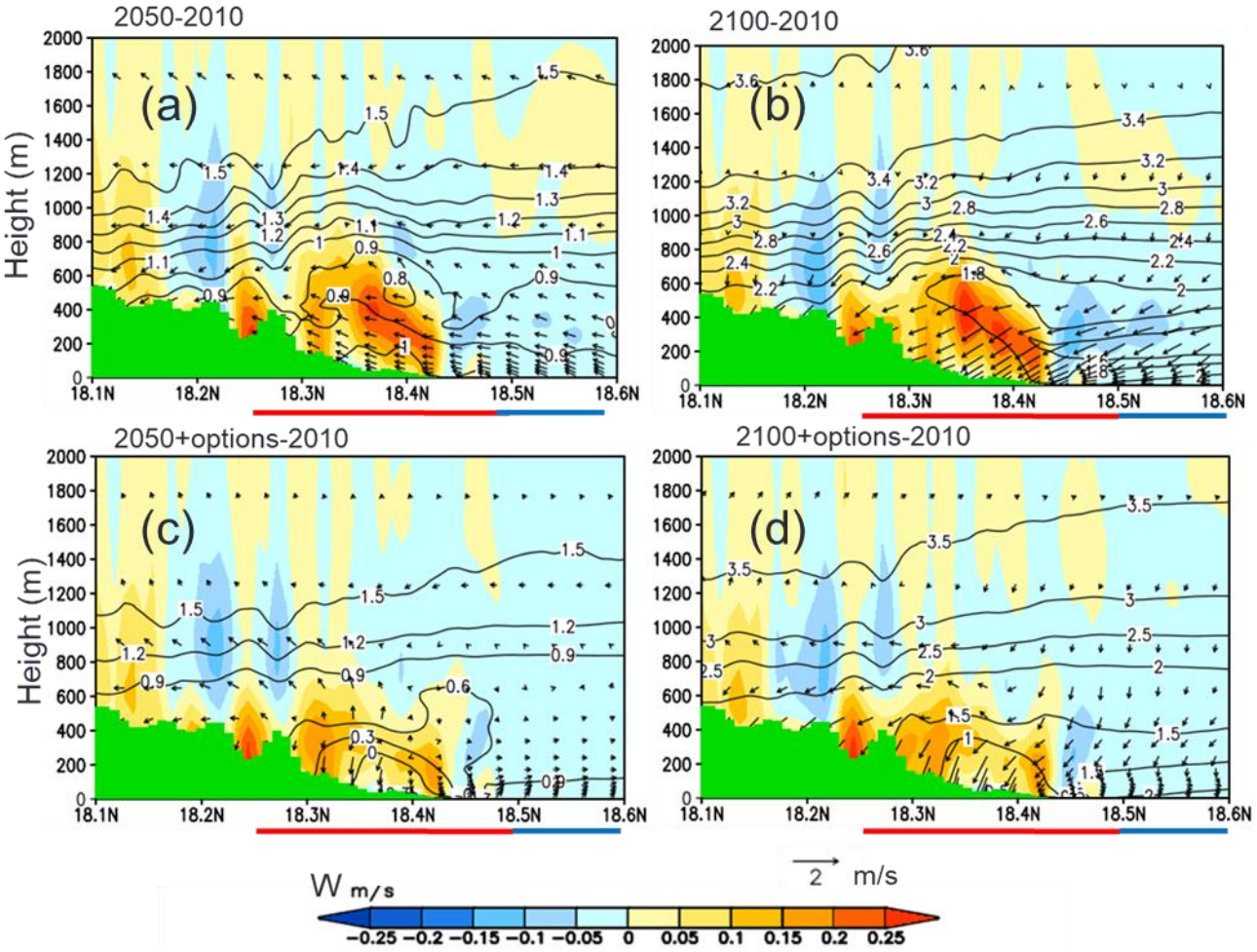

Figure 10. Air temperature difference (contour lines), horizontal wind vector difference, and shaded contour of vertical wind for mean of 18 UTC (2 PM LST). The red line represents urban locations and blue line delineates ocean. The blue shaded colors represent downward vertical motion, whereas the yellow–red shows upward vertical motion. The green filled solid line represents topography. (**a**) contour lines temperature difference (2050–2010) vertical wind difference shaded contours (**b**) temperature difference, wind difference (2100–2010) (**c**) temperature difference, wind difference 2050 with mitigation options—2010 (**d**) temperature difference, wind difference 2100 with mitigation options-2010.

3.6. Model Results for Climate Change Impacts on UHI

The UHI phenomenon can interact with the heat wave or extreme temperature event, and it is one of the most common behaviors reported due to climate change, making the local urban environment warming more lasting and devastating (He Bao-Jie., 2019). For this reason, we studied peak daytime temperatures to evaluate the UHI over the metropolitan region of San Juan passing through −66.1° longitude (shown in Figure 1). The maximum daily UHI intensities for historic, mid- and end-of-century periods are 3 °C, 4 °C, and 5 °C, respectively, representing a climate change signal without building energy mitigation measures (Figure 11). The mitigation measures have the potential of reducing the UHI intensities to 1 °C and 0.5 °C for the 2050 and 2100 climate periods, respectively.

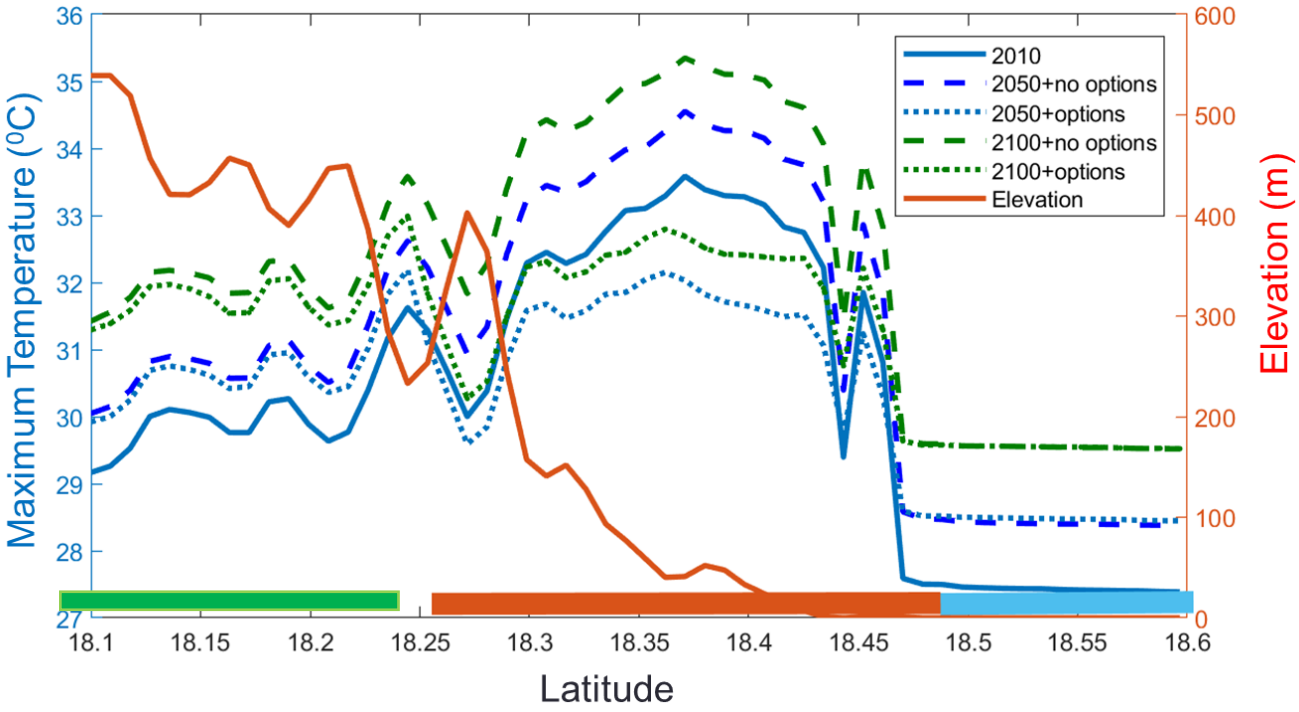

Figure 11. The 2 m air maximum temperature for historic (2010), mid-century, and end-of-century periods with and without mitigation measures passing through −66.1° longitude over San Juan. The thick dark red line indicates urban area, thick blue line indicates ocean, and thick green line indicates rural area.

4. Discussion

An analysis of statistically downscaled global model output for New York shows an underestimation of uncorrected summer daily maximum temperatures, leading to lower heat wave intensity and duration projections, similar to our findings. However, the bias-corrected statistical downscaling reveals much closer results to observation records [58] (Ortiz et al., 2019). High-resolution dynamic downscaling simulations reveal a strong dependency of changes in event duration and intensity on geographical location and urban density. Event intensity changes are expected to be highest closer to the coast, where afternoon sea breezes have traditionally mitigated summer high temperatures. Meanwhile, event intensity is largest over Manhattan (reaching 34.5 °C and 37 °C by 2050 and 2100, respectively), where the urban canopy is denser and taller [58] (Ortiz et al 2019), similar to the SJMA, a coastal metropolitan region of Puerto Rico where heat wave intensity can reach as high as 34 °C and 35 °C for 2050 and 2100, respectively, considering the high-emission (RCP8.5) scenario.

Heat index is an important metric for heat waves in the Caribbean [14,15], which is defined by the correlation between air temperature and humidity. The means of the maximum daily heat index were 31 °C, 32 °C, and 34 °C for the historic period, 2050, and 2100, respectively. The reduction potential with mitigation measures does not reduce the mean maximum heat index value for 2050 and 2100. No change in the heat index with mitigation measures is mainly due to the negative correlation between the 2 m air temperature and humidity, which is also presented in a study by Zeppetello et al., 2022 [60]. Furthermore, Zepetello et al. [60] conclude that half of year will be 'dangerously hot' in the tropics by 2100, where the daily maximum heat index will reach 39.5 °C considering a business-as-usual climate change scenario. A future wind speed projection (2080–2099) of the various cities in the Iberian Peninsula shows that the future horizontal wind will decrease by 0.77 m/s for maximum cities [61]. Our analysis also reveals that wind will decrease by 0.5 m/s by 2050 and 1–1.5 m/s by 2100 for the SJMA considering the RCP8.5 scenario. The results presented here provide useful insights into the interplay between regional and local climate and the potential for localized intensification of extreme heat

events. As cities increase efficacy on greenhouse gas emission reduction efforts, the surrounding ecosystems and natural resources close to urbanized areas are simulated to be affected by climate system changes and variability. These insights may be useful for city-level stakeholders for planning of adaptation strategies for improving population health and energy usage. There are uncertainties in the temporal change in urban parameters such as land cover, building height, or building technologies (e.g., air conditioning efficiency and improved thermal performance), which might modify urban–atmosphere interactions. One particular limitation is the assumption of static urban surface: no urban densification and no change in populations. This limitation might be addressed by the use of future land cover and population projections which could be provided by the policymakers and governmental agencies. Urban densification has shown to contribute to local warming in addition to global climate change in different places around the world, for example, in Paris [62], Tokyo [63], Arizona [64], and Sydney [65]. However, the limitation of data on future urban densification limits the study to some scale when the population projection is significant. This is, however, not the case in the SJMA, as UN population projections of the future are not significantly different from current period.

5. Conclusions

This study investigated the spatio-temporal impacts of climate change in the coastal tropical city of San Juan, Puerto Rico. GCM models without bias correction generally underestimate observations by an average of 5 °C. The statistical downscaling technique (bias correction) modifies each ensemble member's distribution to match that of the station observations more closely. The dynamic downscaling used an urbanized version of WRF, which enabled the exploration of building energy mitigation options (white roof, tilted PV roof, and higher COP). The global climate change signal for the San Juan International Airport indicates an increase in daily maximum temperature by 0.5 °C per decade, and dynamic downscaling results demonstrate that the extreme heat event intensities may reach 35 °C for both mid- and end-of-century periods. The statistical downscaling further shows that the extreme heat events would be more long lasting for the end-of-century period. The dynamic downscaling results show that the extreme heat events are more pronounced in the metropolitan region (urban centers) as a climate change signal for both mid- and end-century periods. However, the combination of the mitigation measures reveals that the extreme heat event frequency is shifted from urban centers to low-level agricultural land and grassland.

The climate change impacts increase the near-surface urban air temperature by 0.9 to 1.1 °C for 2050 and 1.8–2 °C for 2100, respectively, as compared to the historic period. Energy mitigation measures do not show significant differences in temperature over the entire region, except over the urban region where 0–0.3 °C and 1 °C increases are noticed for the 2050 and 2100 periods as compared to the historic period. The horizontal wind speed just over the urban region is seen to decrease by 0.5 m/s and 1–1.5 m/s for 2050 and 2100, respectively, and there are no noticeable changes for 2050 and decreases by 0.5 m/s for 2100 with building energy mitigation measures. The average daily maximum temperature for San Juan indicates that the magnitude is greater than the historic threshold for the 95th percentile (32.8 °C; for extreme heat events) for 2100 (33.2 °C) but slightly lower for 2050 (32.2 °C). These are reduced significantly compared to the threshold with building energy mitigation measures for both periods. Furthermore, the building energy mitigation measures have the potential of reducing the UHI intensities to 1 °C and 0.5 °C for the 2050 and 2100 climate periods, respectively.

Urban densification has shown to contribute to local warming in addition to global climate change in different places around the world, for example, in Paris, Tokyo, Arizona and Sydney. The assumption of considering static land cover land use for future urban densification, as there are no significant changes in population projections (especially for Puerto Rico), is one of the limitations of this study.

Author Contributions: R.P., preparation of the manuscript; J.E.G., revision, editing, and supervising; D.C., revision and editing; P.R., revision and editing. All authors have read and agreed to the published version of the manuscript.

Funding: Financial support for this research was provided by the US National Science Foundation (Grant No. CBET-1438324; Funder ID: 10.13039/100000001), NSF I-CORPS NSF 2018092 and the US Agency for International Development (Grant No. AID-517-A-15-00002; Funder ID: 10.13039/100000200).

Institutional Review Board Statement: Not applicable.

Informed Consent Statement: Not applicable.

Data Availability Statement: Data for all the figures plotted in the manuscript can be provided upon request. Code availability: Matlab and grads code used to plot the data can be provided upon request.

Acknowledgments: The analysis process was conducted at the high-performance computing facilities at the City College of New York (http://cuerg.ccny.cuny.edu/, accessed on 15 January 2023) and the National Center for Atmospheric Research (NCAR) high-performance computing center (https://cunyhpc.csi.cuny.edu/, accessed on 15 January 2023). The US National Science Foundation provided financial support for this research (Grant No. CBET-1438324; Funder ID: 10.13039/100000001), in addition to the US Agency for International Development (Grant No. AID-517-A-15-00002; Funder ID: 10.13039/100000200).

Conflicts of Interest: The article is original and has not been published in any conferences or journals. There is no conflict of interest for this particular manuscript.

Ethics Approval: The manuscript is original and follows ethical standards.

Consent to Participate: Authors are available to participate in the journal program depending on their individual schedule.

Consent for Publication: Authors agree to journal publication charges and other publication requirements.

References

1. Intergovernmental Panel on Climate Change, IPCC. Climate Change, IPCC. Climate Change 2007. The Physical Science Basis. In *Contribution of Working Group I to the Fourth Assessment Report of the Intergovernmental Panel on Climate Change*; Cambridge University Press: Cambridge, UK, 2017.
2. Gamble, D.W.; Curtis, S. Caribbean precipitation: Review, model and prospect. *Prog. Phys. Geogr.* **2008**, *32*, 265–276. [CrossRef]
3. Angeles, M.E.; González, J.E.; Ramírez-Beltrán, N.D.; Tepley, C.A.; Comarazamy, D.E. Origins of the Caribean rainfall bimodal behavior. *J. Geophys. Res. Atmos.* **2010**, 115. [CrossRef]
4. Glenn, E.; Comarazamy, D.; González, J.E.; Smith, T. Detection of recent regional sea surface temperature warming in the Caribbean and surrounding region. *Geophys. Res.* **2015**, *42*, 6785–6792. [CrossRef]
5. Hosannah, N.; González, J.; Rodriguez-Solis, R.; Parsiani, H.; Moshary, F.; Aponte, L.; Armstrong, R.; Harmsen, E.; Ramamurthy, P.; Angeles, M.; et al. The convection, aerosol, and synoptic-effects in the tropics (cast) experiment. *Bull. Amer. Meteorol. Soc.* **2017**, *98*, 1593–1600. [CrossRef]
6. Angeles, E.M.; Gonzalez, J.E.; Ramirez, N. Impacts of climate change on building energy demands in the intra-Americas region. *Theor. Appl. Clim.* **2017**, *133*, 59–72. [CrossRef]
7. Wang, N.; Phelan, P.E.; Gonzalez, J.; Harris, C.; Henze, G.P.; Hutchinson, R.; Langevin, J.; Lazarus, M.A.; Nelson, B.; Pyke, C.; et al. Ten Questions Concerning Future Building Beyond Zero Energy and Carbon Neutrality. *Build. Environ.* **2017**, *119*, 169–182. [CrossRef]
8. González, J.E.; Georgescu, M.; Lemos, M.C.; Hosannah, N.; Niyogi, D. Climate change's pulse is in Central America and the Caribbean. *Eos* **2017**. [CrossRef]
9. Karl, T.R.; Knight, R.W. The 1995 Chicago heat wave:Howl ikely is a recurrence? *Bull. Amer. Meteor. Soc.* **1997**, *78*, 1107–1119. [CrossRef]
10. Delworth, T.L.; Mahlman, J.D.; Knutson, T.R. Changes in Heat Index associated with CO_2-induced global warming. *Clim. Chang.* **1999**, *43*, 369–386. [CrossRef]
11. Deo, R.C.; Mcalpine, C.A.; Syktus, J.; Mcgowan, H.A.; Phinn, S. On Australian Heat Waves: Time Series Analysis of Extreme Temperature Events in Australia, 1950–2005. In Proceedings of the MODSIM 2007 International Congress on Modelling and Simulation, Christchurch, New Zealand, 10–13 December 2007.
12. Robinson, P.J. On the Definition of a Heat Wave. *J. Appl. Meteorol. Climatol.* **2001**, *40*, 762–775. [CrossRef]
13. Fischer, E.M.; Schär, C. Consistent geographical patternsof changes in high-impact European heatwaves. *Nat. Geosci.* **2010**, *3*, 398–403. [CrossRef]
14. Ramirez-Beltran, N.D.; Gonzalez, J.E.; JCastro, J.M.; Angeles, M.; Harmsen, E.W.; Salazar, C.M. Analysis of the heat index in the Mesoamerica and Caribbean region. *J. Appl. Meteorol. Climatol.* **2017**, *56*, 2905–2925. [CrossRef]

15. Angeles-malaspina, M.; González-cruz, J.E.; Ramírez-Beltran, N. Projections of Heat Waves Events in the Intra-Americas Region Using Multimodel Ensemble. *Adv. Meteorol.* **2018**, *2018*, 18–21. [CrossRef]
16. Méndez-Lázaro, P.; Martínez-Sánchez, O.; Méndez-Tejeda, R.; Rodríguez, E.; Morales, E.; Schmit Cortijo, N. Extreme Heat Events in San Juan Puerto Rico: Trends and Variability of Unusual Hot Weather and its Possible Effects on Ecology and Society. *J. Climatol. Weather. Forecast.* **2015**, *3*, 1000135. [CrossRef]
17. Méndez-Lázaro, P.A.; Pérez-Cardona, C.M.; Rodríguez, E.; Martínez, O.; Taboas, M.; Bocanegra, A.; Méndez-Tejeda, R. Climate change, heat, and mortality in the tropical urban area of San Juan, Puerto Rico. *Int. J. Biometeorol.* **2016**, *62*, 699–707. [CrossRef]
18. Li, D.; Bou-Zeid, E. Synergistic interactions between urban heat islands and heat waves: The impact in cities is larger than the sum of its parts. *J. Appl. Meteorol. Climatol.* **2013**, *52*, 2051–2064. [CrossRef]
19. Ramamurthy, P.; González, J.; Ortiz, L.; Arend, M.; Moshary, F. Impact of heatwave on a megacity: An observational analysis of New York City during July 2016. *Environ. Res. Lett.* **2017**, *12*, 054011. [CrossRef]
20. Li, D.; Sun, T.; Liu, M.; Wang, L.; Gao, Z. Changes in wind speed under heat waves enhance urban heat islands in the Beijing Metropolitan Area. *J. Appl. Meteorol. Climatol.* **2016**, *55*, 2369–2375. [CrossRef]
21. Founda, D.; Santamouris, M. Synergies between urban heat island and heat waves in Athens (Greece), during an extremely hot summer (2012). *Sci. Rep.* **2017**, *7*, 10973. [CrossRef]
22. Schatz, J.; Kucharik, C.J. Urban climate effects on extreme temperatures in Madison, Wisconsin, USA. *Environ. Res. Lett.* **2015**, *10*, 094024. [CrossRef]
23. Scott, A.A.; Waugh, D.W.; Zaitchik, B.F. Reduced urban heat island intensity under warmer conditions. *Environ. Res. Lett.* **2018**, *13*, 064003. [CrossRef] [PubMed]
24. He, B.-J. Towards the next generation of green building for urban heat island mitigation: Zero UHI impact building. *Sustain. Cities Soc.* **2019**, *50*, 101647. [CrossRef]
25. United Nations Environment Programme UNEP. Climate Change in Latin America and the Caribbean: Current State and Opportunities. In Proceedings of the 14th Meeting of the Forum of Ministers of the Environment of Latin America and the Caribbean, Panama City, Panama, 20–25 November 2003; Volume 1, pp. 1–27.
26. United Nations Environment Programme UNEP. *Promotion of Newand Renewable Sources of Energy, Including the Implementation of the WorldSolar Programme 1996–2005*; Report of the Secretary General-UNEP; 55th Session; Article 97f; UNEP: Nairobi, Kenya, 2000; pp. 1–7.
27. Reyna, J.; Chester, M. Energy efficiency to reduce residential electricity and natural gas use under climate change. *Nat. Commun.* **2017**, *8*, 14916. [CrossRef] [PubMed]
28. Salamanca, F.; Georgescu, M.; Mahalov, A.; Moustaoui, M.; Martilli, A. Citywide Impacts of Cool Roof and Rooftop Solar Photovoltaic Deployment on Near-Surface Air Temperature and Cooling Energy Demand. *Boundary-Layer Meteorol.* **2016**, *161*, 203–221. [CrossRef]
29. Roman, K.K.; O'Brien, T.; Alvey, J.B.; Woo, O.J. Simulating the Effects of Cool Roof and PCM (Phase Change Materials) Based Roof to Mitigate UHI (Urban Heat Island) in Prominent US Cities. *Energy* **2016**, *96*, 103–117. [CrossRef]
30. Rosenfeld, A.H.; Akbari, H.; Bretz, S.; Fishman, B.L.; Kurn, D.M.; Sailor, D.; Taha, H. Mitigation of urban heat islands: Materials, utility programs, updates. *Energy Build.* **1995**, *22*, 255–2653. [CrossRef]
31. Akbari, H.; Pomerantz, M.; Taha, H. Cool surfaces and shade trees to reduce energy use and improve air quality in urban areas. *Sol. Energy* **2001**, *70*, 295–310. [CrossRef]
32. Oleson, K.W.; Bonan, G.B.; Feddema, J. Effects of White Roofs on Urban Temperature in a Global Climate Model. *Geophys. Res. Lett.* **2010**, *37*, L03701. [CrossRef]
33. Cotana, F.; Rossi, F.; Filipponi, M.; Coccia, V.; Pisello, A.L.; Bonamente, E.; Petrozzi, A.; Cavalaglio, G. Albedo Control as an Effective Strategy to Tackle Global Warming: A Case Study. *Appl. Energy* **2014**, *130*, 641–647. [CrossRef]
34. Ortiz, L.E.; Gonzalez, J.G.; Gutierrez, E.; Arend, M. Forecasting Building Energy Demands with a Coupled Weather-Building Energy Model in a Dense Urban Environment. *J. Sol. Energy Eng.* **2016**, *139*, 011002. [CrossRef]
35. Masson, V.; Bonhomme, M.; Salagnac, J.L.; Briottet, X.; Lemonsu, A. Solar panels reduce both global warming and urban heat island. *Front. Environ. Sci.* **2014**, *2*, 1–10. [CrossRef]
36. Pokhrel, R.; Walker, A.; González, J.E. A new methodology to assess building integrated roof top PV installations at city scales: The tropical coastal city case. *J. Eng. Sustain. Bldgs. Cities* **2020**, *1*, 1–28. [CrossRef]
37. Scherba, A. Modeling the Impact of Roof Reflectivity, Integrated Photovoltaic Panels and Green Roof Systems on the Summertime Heat Island. Master's Thesis, Portland State University, Portland, OR, USA; p. 246. [CrossRef]
38. Pokhrel, R.; Ramirez-Beltran, N.; González, J. On the assessment of alternatives for building cooling load reductions for a tropical coastal city. *Energy Build.* **2019**, *182*, 131–143. [CrossRef]
39. Beccali, M.; Cellura, M.; Lo Brano, V.; Marvuglia, A. Forecasting daily urban electric load profiles using artificial neural networks. *Energy Convers. Manag.* **2004**, *45*, 2879–2900. [CrossRef]
40. Howard, B.; Parshall, L.; Thompson, J.; Hammer, S.; Dickinson, J.; Modi, V. Spatial distribution of urban building energy consumption by end use. *Energy Build.* **2012**, *45*, 141–151. [CrossRef]
41. Ahmed, K.; Ortiz, L.E.; González, J.E. On the Spatio-Temporal End-User Energy Demands of a Dense Urban Environment. *J. Sol. Energy Eng.* **2017**, *139*, 041005. [CrossRef]

42. Olivo, Y.; Hamidi, A.; Ramamurthy, P. Spatiotemporal variability in building energy use in New York city. *Energy* **2017**, *141*, 1393–1401. [CrossRef]
43. Vahmani, P.; Sun, F.; Hall, A.; Ban-Weiss, G. Investigating the climate impacts of urbanization and the potential for cool roofs to counter future climate change in Southern California. *Environ. Res. Lett.* **2016**, *11*, 124027. [CrossRef]
44. Tewari, M.; Salamanca, F.; Martilli, A.; Treinish, L.; Mahalov, A. Impacts of projected urban expansion and global warming on cooling energy demand over a semiarid region. *Atmos. Sci. Lett.* **2017**, *18*, 419–426. [CrossRef]
45. Ortiz, L.E.; Gonzalez, J.; Lin, W. Climate change impacts on peak building cooling energy demand in a coastal megacity. *Environ. Res. Lett.* **2018**, *13*, 94008. [CrossRef]
46. URS. *Fortieth Annual Report on the Electric Property of the Puerto RicoElectric Power Authority*; URS: San Francisco, CA, USA, 2013; pp. 1–132.
47. Reddy, T.A.; Kreider, J.F.; Curtiss, P.S.; Rabl, A. *Heating and Cooling of Buildings: Principles and Practice of Energy Efficient Design*; CRC Press: Boca Raton, FL, USA, 2016.
48. Edwards, E.E.; Iyare, O.S.; Moseley, L.L. Energy consumption in typical Caribbeanoffice buildings: A potential short term solution to energy concerns. *Renew. Energy* **2012**, *39*, 154–161. [CrossRef]
49. Taylor, K.E.; Stouffer, R.J.; Meehl, G.A. An overview of CMIP5 and the Experiment Design. *Bull. Amer. Meteor. Soc.* **2012**, *93*, 485–498. [CrossRef]
50. van Vuuren, D.P.; Edmonds, J.; Kainuma, M.; Riahi, K.; Thomson, A.; Hibbard, K.; Hurtt, G.C.; Kram, T.; Krey, V.; Lamarque, J.-F.; et al. The representative concentration pathways: An overview. *Clim. Chang.* **2011**, *109*, 5–31. [CrossRef]
51. Piani, C.; Weedon, G.P.; Best, M.; Gomes, S.M.; Viterbo, P.; Hagemann, S.; Haerter, J.O. Statistical bias correction of global simulated daily precipitation and temperature for the application of hydrological models. *J. Hydrol.* **2010**, *395*, 199–215. [CrossRef]
52. Hawkins, E.; Osborne, T.M.; Ho, C.K.; Challinor, A.J. Calibration and bias correction of climate projections for crop modelling: An idealised case study over Europe. *Agric. For. Meteorlogy* **2013**, *170*, 19–31. [CrossRef]
53. Bruyère, C.L.; Done, J.M.; Holland, G.J.; Fredrick, S. Bias corrections of global models for regional climate simulations of high-impact weather. *Clim. Dyn.* **2014**, *43*, 1847–1856. [CrossRef]
54. Miller, N.L.; Hayhoe, K.; Jin, J.; Auffhammer, M. Climate, extreme heat, and electricity demand in California. *J. Appl. Meteorol. Climatol.* **2008**, *47*, 1834–1844. [CrossRef]
55. El-Samra, R.; Bou-Zeid, E.; El-Fadel, M. To what extent does high-resolution dynamical downscaling improve the representation of climatic extremes over an orographically complex terrain? *Theor. Appl. Climatol.* **2017**, *134*, 265–282. [CrossRef]
56. Wang, J.; Kotamarthi, V.R. High-resolution dynamically downscaled projections of precipitation in the mid and late 21st century over North America. *Earth's Future* **2015**, *3*, 268–288. [CrossRef]
57. Gao, Y.; Fu, J.S.; Drake, J.B.; Liu, Y.; Lamarque, J.-F. Projected changes of extreme weather events in the eastern United States based on a high-resolution climate modeling system. *Environ. Res. Lett.* **2012**, *7*, 044025. [CrossRef]
58. Ortiz, L.E.; González, J.E.; Horton, R.; Wei, W.L.; Ramamurthy, P.; Arend, M.; Bornstein, R.D. High-resolution projections of extreme heat in New York City. *Int. J. Climatol.* **2019**, *39*, 4721–4735. [CrossRef]
59. Lanzante, J.R.; Dixon, K.W.; Nath, M.J.; Whitlock, C.E.; Adams Smith, D. Some pitfalls in statistical downscaling of future climate. *Bull. Am. Meteorol. Soc.* **2018**, *99*, 791–803. [CrossRef]
60. Zeppetello, L.R.V.; Raftery, A.E.; Battisti, D.S. Probabilistic projections of increased heat stress driven by climate change. *Commun. Earth Environ.* **2022**, *3*, 183. [CrossRef]
61. Martins, J.; Rocha, A.; Viceto, C.; Cardoso, P.S.; Santos, J.A. Future Projections for Wind, Wind Shear and Helicity in the Iberian Peninsula. *Atmosphere* **2020**, *11*, 1001. [CrossRef]
62. Adachi, S.A.; Kimura, F.; Kusaka, H.; Inoue, T.; Ueda, H. Comparison of the impact of global climate. *Natl. Ocean. Atmos. Adm.* **2012**, *23*, 473–493. [CrossRef]
63. Lemonsu, A.; Viguié, V.; Daniel, M.; Masson, V. Vulnerability to heat waves: Impact of urban expansion scenarios on urban heat island and heat stress in Paris (France). *Urban Clim.* **2015**, *14*, 586–605. [CrossRef]
64. Georgescu, M.; Moustaoui, M.; Mahalov, A.; Dudhia, J. Summer-time climate impacts of projected megapolitan expansion in Arizona. *Nat. Clim. Chang.* **2012**, *3*, 37–41. [CrossRef]
65. Argüeso, D.; Evans, J.P.; Fita, L.; Bormann, K.J. Temperature response to future urbanization and climate change. *Clim. Dyn.* **2014**, *42*, 2183–2199. [CrossRef]